Composite Structures 108 (2014) 65–76

Contents lists available at ScienceDirect

Composite Structures

journal homepage: www.elsevier.com/locate/compstruct

Optimal design of rectangular composite flat-panel sound radiators considering excitation location

C.H. Jiang, Y.H. Chang, T.Y. Kam *

Mechanical Engineering Department, National Chiao Tung University, Hsin Chu 300, Taiwan

ARTICLE INFO

Article history:
Available online 14 September 2013

Keywords:
Acoustics
Composite plate
Optimal design
Rayleigh–Ritz method
Sound radiation

ABSTRACT

The optimal excitation locations of rectangular composite sound radiation plates to produce relatively smooth sound level pressure (SPL) curves are determined using an optimal design method. In the optimal design process, the vibration of the plate is analyzed using the Rayleigh–Ritz method, the sound pressure produced by the plate is calculated using the first Rayleigh integral, and the optimal excitation location is determined using a global optimization technique. The experimental SPL curves of several sound radiators were measured to verify the accuracy of the theoretical predictions. In the determination of the optimal excitation location, the trial radius of the circular excitation force is used in the vibro-acoustic analysis to predict the theoretical SPL curve of the plate, a SPL discrepancy function is established to measure the sum of the squared differences between the SPLs at the chosen excitation frequencies and the average value of such SPLs, and a global minimization technique is used to search for the best estimate of the radius of the circular excitation force by making the SPL discrepancy function a global minimum. The optimal excitation locations of several composite sound radiators with different aspect ratios and layups are determined using the proposed method.

1. Introduction

The advantages of composite materials such as high stiffness-to-weight and strength-to-weight ratios have made composite plates find broad applications in different industries such as aero-space, aircraft, automobile, and audio industries to fabricate structures of high performance and reliability. In general, the design of composite plate structures has to tackle the structural vibro-acoustic issue to achieve the goals and functions of these structures. For instance, in the audio industry, composite plates have been used to fabricate composite panel-form sound radiators or speakers for sound radiation. For a panel-form sound radiator/speaker, the sound radiation is induced by the vibration of the plate which is flexibly restrained at its edges and excited by at least one exciter. Therefore, the vibro-acoustics of composite plates has become an important topic of research in the design of composite flat-panel speakers for achieving high quality sound radiation of the speakers. Recently, several researchers have proposed different types of composite panel-form sound radiators [1–7] which may find applications in the consumer electronics. For instance, Guenther and Leigh [1] proposed the use of a composite sandwich sound radiation plate comprising carbon fiber reinforced face sheets and honeycomb core in a flat-panel speaker for attaining improved performance at higher frequencies. Kam [6] proposed the use of a plural number of exciters to excite the composite plate of a panel-form sound radiator at some specific locations to produce a smooth SPL curve for the sound radiator. Since the sound radiation efficiency and quality of a plate are heavily dependent of the vibration characteristics of the plate, the vibro-acoustics of plate structures has thus been studied by many researchers. For instance, many papers [8–20] have been devoted to the vibration and/or sound radiation analyses of plates with different boundary conditions and structural configurations subjected to various types of loads. A number of researchers [21–23] have studied the effects of attached masses on the sound radiation behaviors of plates with regular or flexibly restrained boundary conditions. Regarding the effects of loading conditions on the sound radiation capability of plates, several researchers have studied the SPL curves of plates subjected to different types of loads and excited at various locations [24,25]. As for composite flat-panel sound radiators consisting of one exciter, which may find important applications in the audio industry, no work has been devoted to study how the excitation location affect the sound quality of such sound radiators, not to mention the determination of the optimal excitation locations for the sound radiators. Therefore, the sound radiation behavior of composite flat-panel sound radiation deserves a thorough investigation if flat-panel speakers with good sound quality are to be fabricated.

In this paper, an optimal design method is proposed to determine the optimal excitation locations for composite panel-form

* Corresponding author. Fax: +886 3 6125057.
E-mail address: tykam@mail.nctu.edu.tw (T.Y. Kam).

0263-8223/$ - see front matter © 2013 Elsevier Ltd. All rights reserved.
http://dx.doi.org/10.1016/j.compstruct.2013.09.005

sound radiators consisting of one exciter to possess relatively smooth SPL curves. The vibro-acoustics, especially, the SPL curves of composite panel-form sound radiators are studied via both theoretical and experimental approaches. The Rayleigh–Ritz method together with the first Rayleigh integral is used to study the vibro-acoustic behaviors and construct the SPL curves of the composite plates. The theoretically predicted SPL curves will be verified by the experimental results obtained in this paper. The optimal excitation locations of various sound radiators are determined to produce relatively smooth SPL curves in the given frequency ranges.

2. Plate vibration analysis

In this study, a flat-panel sound radiator consisting of a center exciter is mathematically modeled as an elastically restrained stiffened plate. The stiffened rectangular composite plate of size a (length) $\times$ b (width) $\times$ h_p (thickness) with $a \geqq b$ is elastically restrained along the plate periphery by distributed springs with translational and rotational spring constant intensities K_{Li} and K_{Ri}, respectively, and at the center by a spring of spring constant K_c as shown in Fig. 1. The x–y plane of the global x–y–z coordinate is located at the mid-plane of the symmetrically laminated composite plate which consists of NL orthotropic laminae having different fiber angles with reference to the x-axis. It is noted that the plate is stiffened symmetrically in x and y directions by a number of beams on the bottom surface of the plate. Herein, the displacements of the plate and stiffeners are modeled based on the first-order shear deformation theory [26]. The displacement field of the plate is expressed as

$$\begin{aligned} u_p &= u_{op}(x,y,t) - z_p\theta_{xp}(x,y,t) \\ v_p &= v_{op}(x,y,t) - z_p\theta_{yp}(x,y,t) \\ w_p &= w_{op}(x,y,t) \end{aligned} \tag{1}$$

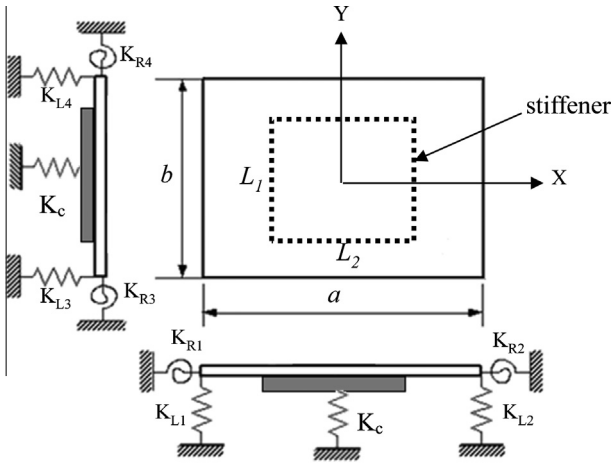

(a) Support condition.

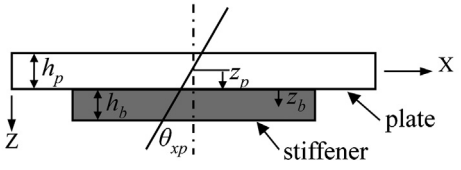

(b) Coordinates.

Fig. 1. Elastically restrained stiffened plate.

where u_p, v_p, and w_p are the displacements in x, y, and z directions, respectively; u_{op}, v_{op}, w_{op} are mid-plane displacements; θ_{xp}, θ_{yp} are shear rotations. It is assumed that both the plate and stiffeners have the same shear rotations. The strain–displacement relations of the plate are expressed as

$$\begin{aligned} \varepsilon_x &= \frac{\partial u}{\partial x} = \frac{\partial u_{op}}{\partial x} + z_p\frac{\partial \theta_{xp}}{\partial x} \\ \varepsilon_y &= \frac{\partial v}{\partial y} = \frac{\partial v_{op}}{\partial y} + z_p\frac{\partial \theta_{yp}}{\partial y} \\ \varepsilon_z &= \frac{\partial w}{\partial z} = \frac{\partial w_{op}}{\partial y} = 0 \\ \gamma_{yz} &= \frac{\partial v}{\partial z} + \frac{\partial w}{\partial y} = \theta_{yp} + \frac{\partial w_{op}}{\partial y} \\ \gamma_{xz} &= \frac{\partial u}{\partial z} + \frac{\partial w}{\partial y} = \theta_{xp} + \frac{\partial w_{op}}{\partial x} \\ \gamma_{xy} &= \frac{\partial u}{\partial y} + \frac{\partial v}{\partial x} = \left(\frac{\partial u_{op}}{\partial y} + \frac{\partial v_{op}}{\partial x}\right) + z_p\left(\frac{\partial \theta_{xp}}{\partial y} + \frac{\partial \theta_{yp}}{\partial x}\right) \end{aligned} \tag{2}$$

The stress–strain relations for the layers in the global x–y–z coordinate system can be expressed in the following general form [27].

$$\begin{Bmatrix} \sigma_x^{(k)} \\ \sigma_y^{(k)} \\ \sigma_z^{(k)} \\ \tau_{yz}^{(k)} \\ \tau_{xz}^{(k)} \\ \tau_{xy}^{(k)} \end{Bmatrix} = \begin{bmatrix} \overline{Q}_{11}^{(k)} & \overline{Q}_{12}^{(k)} & \overline{Q}_{16}^{(k)} & 0 & 0 \\ \overline{Q}_{12}^{(k)} & \overline{Q}_{22}^{(k)} & \overline{Q}_{26}^{(k)} & 0 & 0 \\ \overline{Q}_{16}^{(k)} & \overline{Q}_{26}^{(k)} & \overline{Q}_{66}^{(k)} & 0 & 0 \\ 0 & 0 & 0 & \overline{Q}_{44}^{(k)} & \overline{Q}_{45}^{(k)} \\ 0 & 0 & 0 & \overline{Q}_{45}^{(k)} & \overline{Q}_{55}^{(k)} \end{bmatrix} \cdot \begin{Bmatrix} \varepsilon_x^{(k)} \\ \varepsilon_y^{(k)} \\ \varepsilon_z^{(k)} \\ \gamma_{yz}^{(k)} \\ \gamma_{xz}^{(k)} \\ \gamma_{xy}^{(k)} \end{Bmatrix} \tag{3}$$

where σ, τ are normal and shear stresses, respectively; $\overline{Q}_{ij}^{(k)}$ are the transformed lamina stiffness coefficients which depend on the material properties and fiber orientation of the kth lamina. The relations between the transformed and untransformed lamina stiffness coefficients are expressed as

$$\begin{aligned} \overline{Q}_{11} &= Q_{11}C^4 + 2(Q_{12} + 2Q_{66})C^2S^2 + Q_{22}S^4 \\ \overline{Q}_{12} &= (Q_{11} + Q_{22} - 4Q_{66})C^2S^2 + Q_{12}(C^4 + S^4) \\ \overline{Q}_{16} &= (Q_{11} - Q_{12} - 2Q_{66})C^3S + (Q_{12} - Q_{22} + 2Q_{66})CS^3 \\ \overline{Q}_{22} &= Q_{11}S^4 + 2(Q_{12} + 2Q_{66})C^2S^2 + Q_{22}C^4 \\ \overline{Q}_{26} &= (Q_{11} - Q_{12} - 2Q_{66})CS^3 + (Q_{12} - Q_{22} + 2Q_{66})C^3S \\ \overline{Q}_{66} &= (Q_{11} + Q_{22} - 2Q_{12} - 2Q_{66})C^2S^2 + Q_{66}(C^4 + S^4) \\ \overline{Q}_{44} &= Q_{44}C^2 + Q_{55}S^2, \overline{Q}_{45} = (Q_{55} - Q_{44})CS \\ \overline{Q}_{55} &= Q_{55}C^2 + Q_{44}S^2 \end{aligned} \tag{4a}$$

with

$$\begin{aligned} &Q_{11} = \frac{E_1}{1 - V_{12}V_{21}}; \quad Q_{12} = \frac{V_{12}E_2}{1 - V_{12}V_{21}}; \quad Q_{22} = \frac{E_2}{1 - V_{12}V_{21}} \\ &Q_{44} = G_{23}; \quad Q_{55} = G_{13}; \quad Q_{66} = G_{12}; \quad C = \cos\theta_i, \quad S = \sin\theta_i \end{aligned} \tag{4b}$$

where Q_{ij} are untransformed lamina stiffness coefficients; E_1, E_2 are Young's moduli in the fiber and transverse directions, respectively; V_{ij} is Poisson's ratio for transverse strain in the j-direction when stressed in the i-direction; G_{12} is in-plane shear modulus in the 1–2 plane; G_{12} G_{23} and are transverse shear moduli in the 1–3 and 2–3 planes, respectively; θ_i is the lamina fiber angle of the ith lamina.

The strain energy, U_p, of the plate with volume V_p is

$$U_p = \frac{1}{2}\int_{V_p}(\sigma_x\varepsilon_x + \sigma_y\varepsilon_y + \tau_{xy}\gamma_{xy} + \tau_{xz}\gamma_{xz} + \tau_{zy}\gamma_{zy})dV_p \tag{5}$$

Using the relations in Eqs. (1)–(4) and integrating through the plate thickness, Eq. (5) can be rewritten as

$$
\begin{aligned}
U_P = \frac{1}{2}\int_0^b\int_0^a \Big[& A_{11}u_{0,x}^2 + A_{22}v_{0,y}^2 + 2A_{16}(u_{0,x}u_{0,y} + u_{0,x}v_{0,x}) \\
& + 2A_{26}(v_{0,x}v_{0,y} + u_{0,y}v_{0,y}) + 2A_{12}u_{0,x}v_{0,y} \\
& + A_{66}(u_{0,y} + v_{0,x})^2 + A_{45}(\theta_{yp} + w_{,y})(\theta_{xp} + w_{,x}) \\
& + A_{44}(\theta_{yp} + w_{,y})^2 + A_{55}(\theta_{xp} + w_{,x})^2 \\
& + 2B_{11}u_{0,x}\theta_{xp,x} + 2B_{22}v_{0,y}\theta_{yp,y} \\
& + 2B_{16}(u_{0,x}\theta_{xp,y} + v_{0,x}\theta_{xp,x} + u_{0,x}\theta_{yp,x} + u_{0,y}\theta_{xp,x}) \\
& + 2B_{26}(v_{0,x}\theta_{yp,y} + u_{0,y}\theta_{yp,y} + v_{0,y}\theta_{xp,y} + v_{0,y}\theta_{yp,x}) \\
& + 2B_{12}(u_{0,x}\theta_{yp,y} + v_{0,y}\theta_{xp,x}) \\
& + 2B_{66}(v_{0,x}\theta_{yp,x} + u_{0,y}\theta_{yp,x} + v_{0,x}\theta_{xp,y} + u_{0,y}\theta_{xp,y}) \\
& + D_{11}\theta_{xp,x}^2 + D_{22}\theta_{yp,y}^2 + 2D_{12}\theta_{xp,x}\theta_{yp,y} \\
& + 2D_{16}(\theta_{xp,x}\theta_{yp,x} + \theta_{xp,x}\theta_{xp,y}) + 2D_{26}(\theta_{yp,y}\theta_{yp,x} + \theta_{yp,y}\theta_{xp,y}) \\
& + D_{66}(\theta_{xp,y} + \theta_{yp,x})^2\Big]dxdy
\end{aligned} \tag{6}
$$

where the subscript comma denotes derivative; A_{ij}, B_{ij}, and D_{ij} are material components which are given by

$$
(A_{ij}, B_{ij}, D_{ij}) = \int_{\frac{-h}{2}}^{\frac{h}{2}} \overline{Q}_{ij}^{(m)}(1, z, z^2)dz, \quad (i,j = 1,2,6) \tag{7}
$$

and

$$
A_{ij} = k_\alpha \cdot k_\beta \cdot \overline{A}_{ij}, \quad \overline{A}_{ij} = \int_{\frac{-h}{2}}^{\frac{h}{2}} \overline{Q}_{ij}^{(m)}\, dz
$$

$$
(\alpha = 6 - i, \beta = 6 - j), \quad (i,j = 4,5)
$$

where k_α is shear correction factor which can be evaluated from the following expressions given by Whitney [28].

$$
k_1^2 = \left[A_{55}\int_{\frac{-t}{2}}^{\frac{t}{2}} g_1^{(m)}(z)\, dz\right]^{-1} \tag{8a}
$$

and

$$
k_2^2 = \left[A_{44}\int_{\frac{-t}{2}}^{\frac{t}{2}} g_2^{(m)}(z)\, dz\right]^{-1} \tag{8b}
$$

with

$$
g_1^{(m)} = S_{55}^{(m)}\left[a^{(m)} + \overline{Q}_{11}^{(m)} \cdot z(2B_{11} - A_{11}z)/2D\right]^2 \tag{9a}
$$

and

$$
g_2^{(m)} = S_{44}^{(m)}\left[a^{(m)} + \overline{Q}_{22}^{(m)} \cdot z(2B_{22} - A_{22}z)/2D\right]^2 \tag{9b}
$$

where

$$
D = \left(D_{11}A_{11} - B_{11}^2\right) \tag{9c}
$$

In Eq. (9), $a^{(m)}$ are constants determined from interface continuity conditions and the requirement that transverse shear stress vanish on the bottom surface of the plate; $S_{44}^{(m)}$ and $S_{55}^{(m)}$ are the shear compliances. It has been shown that the use of the above exact expressions for evaluating shear correction factors in the vibration and buckling analyses of cross-ply and angle-ply composite plates can yield very good results, as demonstrated in Refs. [29–31].

The kinetic energy, T_p, of the plate is

$$
T_p = \frac{1}{2}\int_{V_p} \rho_p\left(\dot{u}_p^2 + \dot{v}_p^2 + \dot{w}_p^2\right)dV_p \tag{10}
$$

where ρ_p is plate mass density. In view of Eq. (1), the above equation can be rewritten as

$$
T_P = \frac{1}{2}\int_0^a\int_0^b \rho_p\left[h_p\left(\frac{\partial u_{op}}{\partial t}\right)^2 + \frac{1}{2}\frac{h_p^3}{12}\left(\frac{\partial \theta_{xp}}{\partial t}\right)^2 + h_p\left(\frac{\partial v_{op}}{\partial t}\right)^2 + \frac{h_p^3}{12}\left(\frac{\partial \theta_{yp}}{\partial t}\right)^2 + h_p\left(\frac{\partial w_{op}}{\partial t}\right)^2\right]dx\,dy \tag{11}
$$

Considering the deformation of the stiffeners, the displacement field of a typical stiffener, for instance, a bottom stiffener oriented in x-direction is:

$$
\begin{aligned}
u_{b_3} &= u_{op}(x,t) + \frac{h_p}{2}\theta_{xp}(x,t) + z_b\theta_{xp}(x,t) \\
v_{b_3} &= 0 \\
w_{b_3} &= w_{op}(x,t)
\end{aligned} \tag{12}
$$

where u_b, v_b, w_b are stiffener displacements. Here the lateral displacement of the stiffener is neglected and treated as zero. The strains and strain energy of the stiffener are given, respectively, as

$$
\begin{aligned}
\varepsilon_x &= \frac{\partial u}{\partial x} = \frac{\partial u_{op}}{\partial x} + \frac{h_p}{2}\frac{\partial \theta_{xp}}{\partial x} + z_b\frac{\partial \theta_{xp}}{\partial x} \\
\varepsilon_y &= 0 \\
\varepsilon_z &= 0 \\
\gamma_{yz} &= 0 \\
\gamma_{xz} &= \frac{\partial u}{\partial z} + \frac{\partial w}{\partial x} = \theta_{xp} + \frac{\partial w_{op}}{\partial x} \\
\gamma_{xy} &= 0
\end{aligned} \tag{13}
$$

and

$$
\begin{aligned}
U_b = \int_{\frac{-L_b}{2}}^{\frac{L_b}{2}} \Big[& \frac{1}{2}E_b h_b t_b\left(\frac{\partial u_{op}}{\partial x}\right)^2 + \frac{1}{8}E_b h_p^2 h_b t_b\left(\frac{\partial \theta_{xp}}{\partial x}\right)^2 \\
& + \frac{1}{6}E_b h_b^3 t_b\left(\frac{\partial \theta_{xp}}{\partial x}\right)^2 + \frac{1}{2}E_b h_p t_b h_b\left(\frac{\partial u_{op}}{\partial x}\right)\left(\frac{\partial \theta_{xp}}{\partial x}\right) \\
& + \left(\frac{\partial \theta_{xp}}{\partial x}\right) - \frac{1}{2}t_b E_b h_b^2\left(\frac{\partial u_{op}}{\partial x}\right)\left(\frac{\partial \theta_{xp}}{\partial x}\right) \\
& + \frac{1}{4}E_b h_p t_b h_b^2\left(\frac{\partial \theta_{xp}}{\partial x}\right)^2 + \frac{1}{2}K_b G_b t_b h_b \theta_{xp}^2 \\
& + K_b G_b t_b h_b \theta_{xp}^2\left(\frac{\partial w_{op}}{\partial x}\right) + \frac{1}{2}K_b G_b t_b h_b\left(\frac{\partial w_{op}}{\partial x}\right)^2 \\
& + \frac{1}{3}G_b h_b t_b^3\left(\frac{\partial w_{op}}{\partial y}\right)^2\Big]dx
\end{aligned} \tag{14}
$$

where E_b is stiffener Young's modulus, L_b length, h_b height, t_b thickness, G_b shear modulus, and K_b shear correction factor. Here, without loss of generality and causing much adverse effects on plate responses, it is assumed that $K_b = 5/6$. The kinetic energy of the stiffener is

$$
T_b = \frac{1}{2}\int_{V_b} \rho_b\left[\left(\frac{\partial u_{op}}{\partial t} - \frac{h_p}{2}\frac{\partial \theta_{xp}}{\partial t} + z_b\frac{\partial \theta_{xp}}{\partial t}\right)^2 + \left(\frac{\partial w_{op}}{\partial t}\right)^2\right]dV_b \tag{15}
$$

where ρ_b is stiffener mass density.

The strain energy, U_S, stored in the elastic restraints is written as

$$
\begin{aligned}
U_S = & \frac{K_{L1}}{2}\int_0^b w^2|_{x=0}\, dy + \frac{K_{L2}}{2}\int_0^b w^2|_{x=a}\, dy \\
& + \frac{K_{L3}}{2}\int_0^a w^2|_{y=0}\, dx + \frac{K_{L4}}{2}\int_0^a w^2|_{y=b}\, dx \\
& + \frac{K_{R1}}{2}\int_0^b (\theta_{xp})^2|_{x=0}\, dy + \frac{K_{R2}}{2}\int_0^b (\theta_{xp})^2|_{x=a}\, dy \\
& + \frac{K_{R3}}{2}\int_0^a (\theta_{yp})^2|_{y=0}\, dx + \frac{K_{R4}}{2}\int_0^a (\theta_{yp})^2|_{y=b}\, dx \\
& + \frac{1}{2}K_C w\left(\frac{a}{2}, \frac{b}{2}\right)^2
\end{aligned} \tag{16}
$$

It is noted that since the interior support is relatively flexible, the use of a spring is sufficient to simulate the effects of the interior support on the dynamic behavior of the plate. The total strain energy U and total kinetic energy T of the elastically restrained stiffened plate are written, respectively, as

$$U = U_p + \sum_{i=1}^{N_b} U_{bi} + U_S \tag{17}$$

and

$$T = T_p + \sum_{i=1}^{N_b} T_{bi} \tag{18}$$

where N_b is number of stiffeners.

The Rayleigh–Ritz method is used to study the free vibration of the elastically restrained stiffened plate. The displacements of the plate are expressed as

$$\begin{aligned} u_0(x,y,t) &= U(x,y)\sin\omega t \\ v_0(x,y,t) &= V(x,y)\sin\omega t \\ w_0(x,y,t) &= W(x,y)\sin\omega t \\ \theta_x(x,y,t) &= \Theta_x(x,y)\sin\omega t \\ \theta_y(x,y,t) &= \Theta_y(x,y)\sin\omega t \end{aligned} \tag{19}$$

with

$$\begin{aligned} U(\xi,\eta) &= \sum_{i=1}^{\widehat{A}}\sum_{j=1}^{\widehat{B}} C_{ij}\phi_i(\xi)\psi_j(\eta) \\ V(\xi,\eta) &= \sum_{i=1+\widehat{A}}^{\widehat{C}}\sum_{j=1+\widehat{B}}^{\widehat{D}} C_{ij}\phi_i(\xi)\psi_j(\eta) \\ W(\xi,\eta) &= \sum_{i=1+\widehat{C}}^{\widehat{I}}\sum_{j=1+\widehat{D}}^{\widehat{J}} C_{ij}\phi_i(\xi)\psi_j(\eta) \\ \Theta_x^{(1)}(\xi,\eta) &= \sum_{i=1+\widehat{I}}^{\widehat{M}}\sum_{j=1+\widehat{J}}^{\widehat{N}} C_{ij}\phi_i(\xi)\psi_j(\eta) \\ \Theta_y^{(1)}(\xi,\eta) &= \sum_{i=1+\widehat{M}}^{\widehat{P}}\sum_{j=1+\widehat{N}}^{\widehat{Q}} C_{ij}\phi_i(\xi)\psi_j(\eta) \end{aligned} \tag{20}$$

where C_{ij} are unknown constants. Legendre's polynomials are used to represent the characteristic functions, ϕ and ψ. Let $\xi = (2x/a) - 1$ and $\eta = (2y/b) - 1$. The normalized characteristic functions, for instance, $\phi_{(i)}(\xi)$, are given as

$$\begin{aligned} &\phi_1(\xi) = 1, \\ &\phi_2(\xi) = \xi, \quad -1 \leqslant \xi \leqslant 1 \end{aligned} \tag{21}$$

for $n \geqslant 3$,

$$\phi_n(\xi) = [(2n-3)\xi \times \phi_{n-1}(\xi) - (n-2)\times\phi_{n-2}(\xi)]/(n-1)$$

with the satisfaction of the following orthogonality condition:

$$\int_{-1}^{1} \phi_n(\xi)\phi_m(\xi)d\xi = \begin{cases} 0 & , \text{ if } n \neq m \\ 2/(2n-1) & , \text{ if } n = m \end{cases} \tag{22}$$

Extremization of the functional $\Pi = T - U$ gives the following eigenvalue problem.

$$[\mathbf{K} - \omega^2\mathbf{M}]\mathbf{C} = 0 \tag{23}$$

where $\mathbf{K}$ and $\mathbf{M}$ are structural stiffness and mass matrices; ω is circular frequency. The solution of the above eigenvalue problem can lead to the determination of the natural frequencies and mode shapes of the stiffened plate. The terms in $\mathbf{K}$ and $\mathbf{M}$ are listed in the appendix.

3. Plate sound radiation analysis

The equations of motion for the sound radiation plate subjected to forced vibration derived via a variational approach can be expressed in the following algebraic form.

$$\mathbf{M}\ddot{\mathbf{C}} + \mathbf{D}\dot{\mathbf{C}} + \mathbf{K}\mathbf{C} = \mathbf{F} \tag{24}$$

where $\mathbf{F}$ is the force vector and $\mathbf{D}$ is damping matrix. For a sound radiation panel excited by an electro-magnetic transducer with a cylindrical voice coil, the harmonic driving force $F(t) = F_o\sin\omega t$ is distributed uniformly around the periphery of the voice coil. The amplitude of the harmonic force is $F_o = BLI$ with B = magnetic flux, L = wire length, and I = electric current. The force vector $\mathbf{F}$ then contains the following terms.

$$\begin{aligned} F_{mn} &= \frac{F_o}{2\pi r_C}\int_0^{2\pi} \phi_m\left(\frac{2r_C}{a}\cos\theta\right)\varphi_n\left(\frac{2r_C}{b}\cos\theta\right)d\theta\sin\omega t, \\ &\quad \text{for } m = 1+\widehat{C},\ldots,\widehat{I}; \quad n = 1+\widehat{D},\ldots,\widehat{J} \\ &= 0 \quad \text{for other } i,j \end{aligned} \tag{25}$$

The damping of the sound radiator is assumed to be proportional.

$$[\mathbf{D}] = \alpha[\mathbf{M}] + \beta[\mathbf{K}] \tag{26}$$

with $\alpha = \zeta\omega$ and $\beta = 2\zeta/\omega$ where ζ is damping ratio at the first resonant frequency of the elastically restrained plate. Eq. (24) can be solved using the modal analysis method.

Referring to the baffled plate with area S shown in Fig. 2, if the effects of air loading on the plate vibration are neglected, the sound pressure $p(r, t)$ resulting from the c of the plate can be determined using the first Rayleigh integral.

$$p(r,t) = \frac{-\omega^2\rho_0}{2\pi}\sum_i A_i e^{j(2\omega t+\theta i - kr_i)}\frac{\Delta S_i}{R_i} \tag{27}$$

where ρ_0 is air density; k is wave number ($=\omega/c$) with c being speed of sound; r_p is the distance between the plate center and the point of measurement; $R_i = |r_p - r_i|$ the distance between the observation point and the position of the surface element at r_i; θ is phase angle; ΔS_i is differential area; $j = \sqrt{-1}$. For air at 20 °C and standard atmospheric pressure, $\rho_0 = 1.2$ kg/m^3 and $c = 344$ m/s. The SPL produced by the plate is calculated as

$$SPL \equiv 20\log_{10}\left(\frac{p_{rms}}{2\times10^{-5}}\right)\ dB \tag{28}$$

with

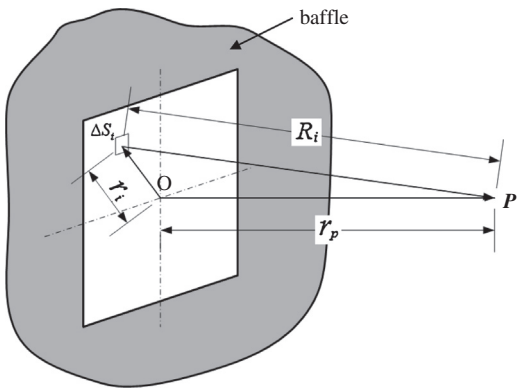

Fig. 2. Sound pressure measurement of baffled plate.

$$p_{rms} = \left[\frac{1}{T}\int_{-T/2}^{T/2} |p(r,t)|^2 dt\right]^{1/2} \tag{29}$$

It is noted that both Eqs. (27) and (29) are calculated numerically.

4. Optimal excitation location

For a sound radiator having good sound quality, it is essential that the SPL curve of the sound radiator be relatively smooth. Therefore, one of the objectives in designing a sound radiator for attaining high sound quality is to make the sound radiator possess a relatively smooth SPL curve. Herein, the problem of determining the optimal size of the circular excitation force for a laminated composite sound radiator to produce a smooth SPL curve in a specific frequency range, $[f_L, f_U]$, is formulated as the following minimization problem.

$$\begin{aligned} &\textit{Minimize}: \quad e(r_c) = \min \sum_{n=1}^{Nf} (S_n - S_a)^2 \\ &\textit{Subject to}: \quad r_c^L \leqslant r_c \leqslant r_c^U \\ &\textit{with} \qquad\quad S_a = \frac{\sum_{n=1}^{Nf} S_n}{Nf} \end{aligned} \tag{30}$$

where S_n are SPLs at the chosen frequencies in the given frequency range; Nf is number of chosen frequencies; S_a is the average of the predicted SPLs at the chosen frequencies; $e(r_c)$ is the deviation function measuring the sum of the square differences between the chosen SPLs and S_a; r_c^L and r_c^U are the lower and upper bounds of the radius of the circular force, respectively. In general, the length of the short side of the plate is set as r_c^U while the radius of the magnet of the exciter is set as r_c^U. Without loss of generality, the frequency range, $[f_L, f_U]$, considered in the optimal design covers the frequency of one of the major SPL dips. For instance, consider the frequency of the first major SPL dip f_{1s}. The distance between any two neighboring sample frequencies, which are less than or equal to f_{1s}, is calculated as $(f_{1s} - f_L)/\alpha$ where α is number of intervals on the left of f_{1s}. Similarly, the distance between any two neighboring sample frequencies, which are larger than or equal to f_{1s}, is calculated as $(f_U - f_{1s})/(Nf - \alpha - 1)$. The above problem of Eq. (30) is then converted into an unconstrained minimization problem by creating the following general augmented Lagrangian.

$$\overline{\Psi}(r_c, \mu, \eta, r_p) = e(r_c) + (\mu\tilde{z} + r_p\tilde{z}^2 + \eta\phi + r_p\phi^2) \tag{31}$$

with

$$\begin{aligned} &\tilde{z} = \max\left[g(r_c), \frac{-\mu}{2r_p}\right] \\ &g(r_c) = r_c - r_c^U \leqslant 0 \\ &\phi = \max\left[H(r_c), \frac{-\mu}{2r_p}\right] \\ &H(r_c) = r_c^L - r_c \leqslant 0 \end{aligned} \tag{32}$$

where μ, η, r_p are multipliers; max[$*$, $*$] takes on the maximum value of the numbers in the bracket. The previously proposed stochastic global optimization method [32–34] is then used to solve the above unconstrained minimization problem to find the best estimate of the radius of the circular load. It is noted that in the adopted optimization method several starting points are randomly generated and for each starting point the lowest local minimum is searched. The solution converges when the probability of obtaining the global minimum reaches 0.95.

5. Experimental investigation

The sound radiation characteristics of two square panel-form sound radiators, namely, Radiators A and B, consisting of $[0°]_4$ Carbon/Epoxy laminated composite plates of lengths 110 mm and 30 mm, respectively, were investigated experimentally. In each sound radiator, the plate used for sound radiation was peripherally suspended by a flexible surround and excited at the plate center by a circular electro-magnetic type exciter. The material properties of the Carbon/Epoxy lamina determined experimentally are given as follows.

$$\begin{aligned} &E_1 = 115.05\ \text{GPa}, \quad E_2 = 7.870\ \text{GPa}, \quad \nu_{12} = 0.306, \quad \nu_{23} = 0.250, \\ &\nu_{13} = 0.306, \\ &G_{12} = 4.10\ \text{GPa}, \quad G_{23} = 0.674\ \text{GPa}, \quad G_{13} = 4.10\ \text{GPa}, \\ &\rho = 1403\ \text{kg/m}^3, \quad t = 0.145\ \text{mm} \end{aligned} \tag{33}$$

The voice coil of the exciter was adhesively attached to the bottom surface of the plate. The properties of the exciter are given as follows.

Voice coil:

$$\begin{aligned} &r_c = 12.75\ \text{mm}, \quad h_b = 20\ \text{mm}, \quad t_b = 0.15\ \text{mm}, \quad \text{E} = 0.159\ \text{GPa}, \\ &\nu = 0.33, \quad \rho = 5763\ \text{kg/m}^3, \quad L = 7.63 \times 10^3\ \text{mm}, \quad \text{R} = 8\ \text{Ohm} \end{aligned} \tag{34}$$

Magnetic assembly:

$$B = 0.263\ \text{Guass} \tag{35}$$

The experimental setup for measuring the sound radiation of the plate is shown schematically in Fig. 3 and the test was conducted in a semi-anechoic chamber. The sound pressure generated from the plate under an input electric power of one Watt was measured using a microphone placed at a location one meter directly from the center of the front surface of the sound radiator. The sound pressure signals were then processed using LMS [35] to produce the SPL curve of the plate.

6. Results and discussions

The proposed method is first applied to the prediction of the SPL curves of the composite flat-panel sound radiators which have been tested. In this study, the voice coil of each sound radiator is modeled using four beam-type stiffeners. The stiffeners of cross-sectional size $2.0 \times 0.15\ \text{mm}^2$ used to model the voice coil have their end points located, respectively, at [10.01,10.01], [−10.01,10.01], [10.01,−10.01], and [−10.01,−10.01] mm. It is noted that the perimeter of the voice coil is the same as the total length of the four beams. In using the present Rayleigh–Ritz

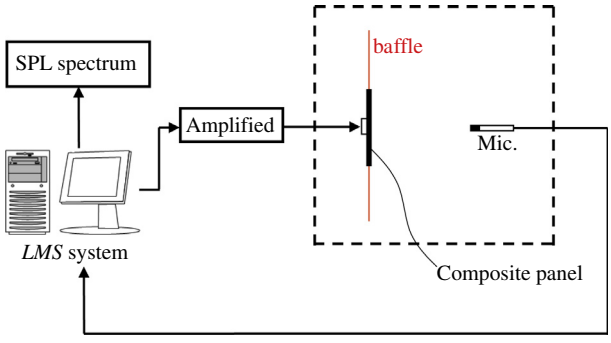

Fig. 3. Sound measurement apparatus.

method for free vibration analysis of the sound radiators, the convergence test has shown that the use of 15 terms of the characteristic functions for each displacement components to predict the natural frequencies of the radiators below 5 kHz can produce acceptable results with errors less than 6% when compared with the finite element solutions obtained using the commercial code ANSYS [36]. It is noted that in the finite element formulation of the flat-panel sound radiator, plate elements (Shell 99) have been used to model the plate as well as the voice coil and spring elements (Combin 4) to model the flexible surround [37]. First consider the SPL curve of Radiator A with peripheral spring constant intensity $K_L = 2030.52$ N/m^2 and central spring constant intensity $K_C = 807.10$ N/m^2. The experimental and theoretical SPL curves of the sound radiator in the frequency range below 3 kHz are shown in Fig. 4 for comparison. It is noted that both SPL curves are in fairly good agreement. In particular, the first and second major dips of the theoretical SPL at 180 and 600 Hz, respectively, can approximately match their experimental counterparts at 180 and 630 Hz, respectively. The discrepancies between the two SPL curves may be due to the uncertainties in the properties of the sound radiator. It is also noted that the first and second major SPL dips of magnitudes 10 and 7 dB, respectively, are induced by the second and fourth modes, respectively, as shown in Fig. 5. For instance, considering the first major SPL dip caused by the 2nd mode shape, it is noted that the plate is symmetrically divided into two regions of opposite phases, namely, the end and center regions and the interference of the sounds radiated from these regions is the cause of the SPL dip. Next, consider the SPL curve of Radiator B with peripheral spring constant intensity $K_L = 906.6$ N/m^2 and central spring constant intensity $K_C = 807.10$ N/m^2. The experimental and theoretical SPL curves of the sound radiator in the frequency range below 3 kHz are shown in Fig. 6 for comparison. Again, it is noted that both SPL curves are in good agreement and the discrepancies between the two SPL curves may be due to the uncertainties in the properties of the sound radiator. It is also worthy to note that the first major SPL dip associated with the 2nd mode shape as well as the other SPL dips in the higher frequency range which have occurred on the SPL curve of Radiator A disappear in this case. The reason for obtaining a relatively smooth SPL curve for Radiator B will be explained in the optimal design of flat-panel sound radiators as described subsequently.

The optimal design of Radiator A is first considered. The parameters used in the optimal design are given as

$$f_L = 100 \text{ Hz}, \quad f_U = 1.5 \text{ kHz}, \quad x_j^L = 12.75 \text{ mm},$$
$$x_j^U = 110 \text{ mm}, \; Nf = 8, \; \alpha = 2$$

The radius of the optimal excitation location has been obtained as $r_{co} = 51.65$ mm and the ratio of optimal voice coil diameter to plate width is $2r_{co}/b = 0.94$. The SPL curve of the sound radiator excited at the optimal excitation location is shown in Fig. 7 in comparison with the experimental SPL curve of the original design. It is noted that the SPL curve of the optimal design becomes much smoother than the one of the original design. In particular, on the optimal SPL curve, the first major SPL dip at 180 Hz disappears and the magnitude of the second major one at 600 Hz becomes approximately 2 dB comparing with the 8 dB drop of the original SPL curve. The vibration shapes of the plate at the two major SPL dip frequencies before and after the optimal design process are listed in Table 1 for comparison. It is noted that the original vibration shapes are similar to the mode shapes of the plate before optimization. These vibration shapes, however, change when the plate is excited at the optimal location. The shape changes imply the suppression of the mode shapes which are detrimental to sound

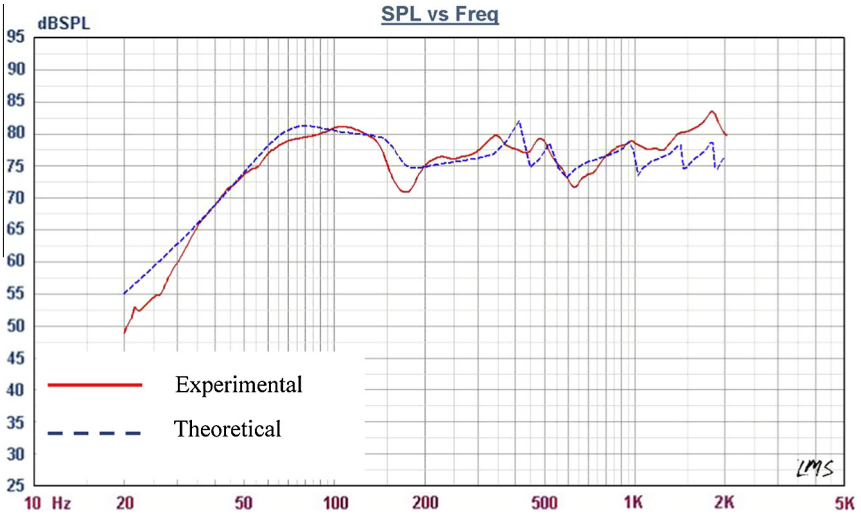

Fig. 4. Theoretical and experimental SPL curves of Carbon/Epoxy $[0°]_4$ plate (Radiator A).

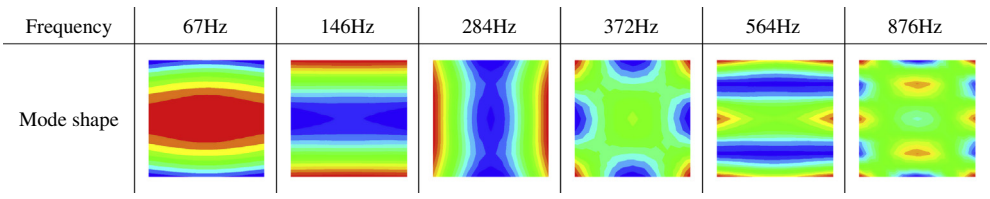

Fig. 5. Mode shape associated with SPL dip of Radiator A.

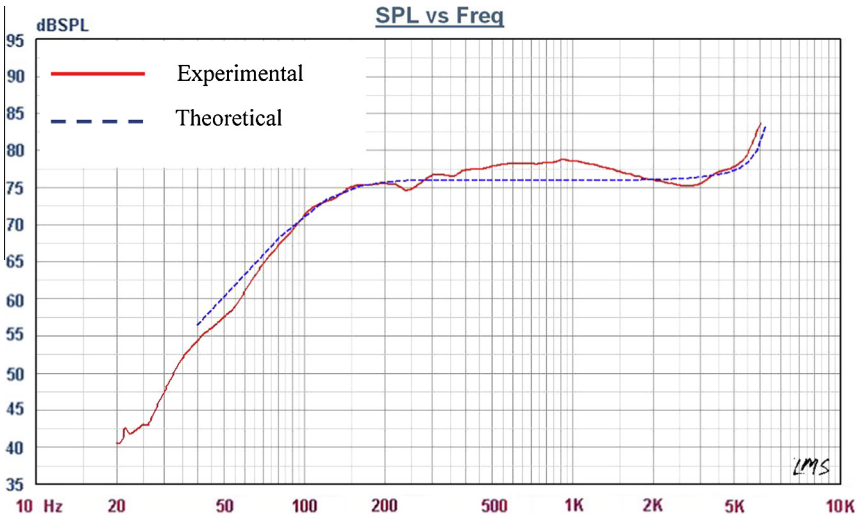

Fig. 6. Theoretical and experimental SPL curves of Carbon/Epoxy $[0°]_4$ plate (Radiator B).

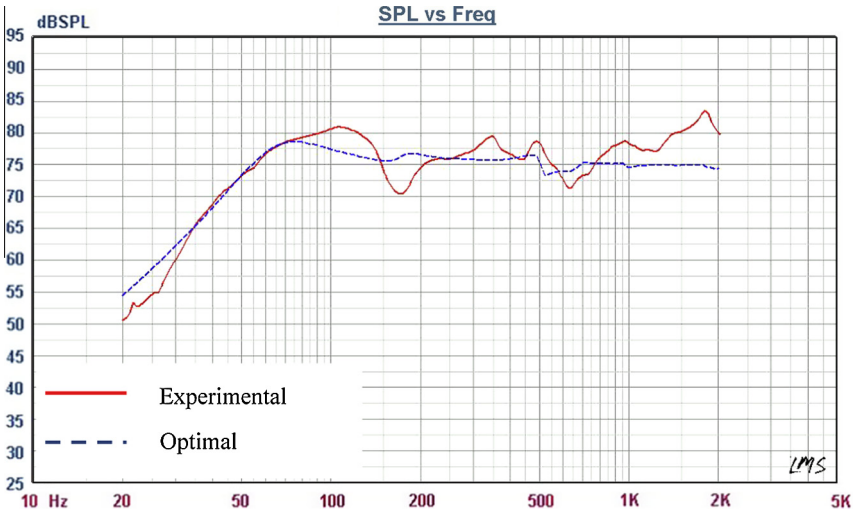

Fig. 7. SPL curves of Radiator A excited at the different locations.

radiation. For illustration purpose, the excitation locations are also plotted as dotted circles on the vibration shapes before and after optimization, respectively, in the figure. In particular, for the vibration shape (2nd mode shape) associated with the first major SPL dip, it is noted that the nodal lines of the shape intersect the y-axis at two nodes with $y = 33.5$ mm and -33.5 mm, respectively, and the shortest distance between each node and the excitation location (voice coil) changes from 20.75 mm before optimization to -18.125 mm after optimization. The meaning of negative distance is that the nodes are inside the circular force. Such excitation location change helps suppress the detrimental effects on the sound radiation of the plate at that frequency and thus improve the smoothness of the SPL curve.

Next consider the optimal design of Radiator B. The parameters used in the design are given as

$$f_L = 150\,\text{Hz},\ \ f_U = 2\,\text{kHz},\ \ x_j^L = 10\,\text{mm},\ \ x_j^L = 30\,\text{mm},\ Nf = 5,\ \alpha = 2$$

The radius of the optimal excitation location has been obtained as $r_{co} = 13.32$ mm and the ratio of optimal voice coil diameter to plate width is $2r_{co}/b = 0.89$. The SPL curve of the sound radiator with the optimal excitation location is shown in Fig. 8 to compare with the experimental one produced by Radiator B. It is noted that the close agreement between the two SPL curves is due to the fact that the initial excitation location is very close to the optimal one. For comparison purpose, the SPL curve of the sound radiator excited by a voice coil of radius $r_c = 6$ mm is also shown in the figure. It is noted that when the radius becomes small, a big dip is induced on the SPL curve at around 1.6 kHz. The vibration shapes excited at different locations are also listed in Table 2 with the dotted circles denoting the excitation locations. It is noted that if the sound radiator is not proper excited such as the case of $r_c = 6$ mm, big dips may be induced on the SPL curve. As for the case of optimal excitation location, the actual vibration shapes are different from the mode shapes which can cause SPL dips. These shape differences thus imply the suppression of all the mode shapes detrimental to sound radiation in the chosen frequency range.

The optimal excitation locations of Radiator A with different aspect ratios or lamination arrangements are determined using the proposed optimal design method. First, consider the effects of aspect ratio on the optimal excitation location of the sound radiator. The optimal radii of the excitation locations for the sound radiators with aspect ratios of $a/b = 1.25$ and 1.6, under the condition that the areas of these plates are equal to that of Radiator A, are

Table 1
Vibration shapes of Radiator A with different voice coil radii.

Frequency (Hz)	Vibration shape (r_c = 12.75 mm)	r_{co} = 51.65 mm
180	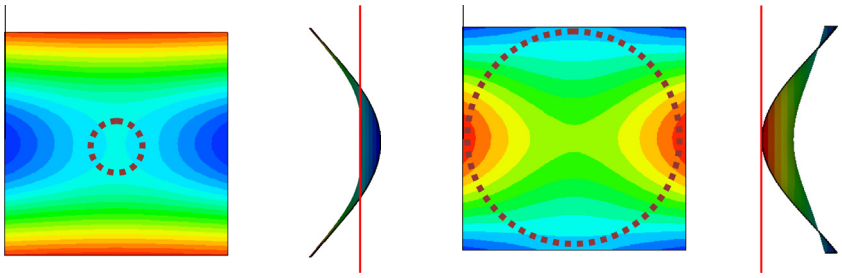	
600	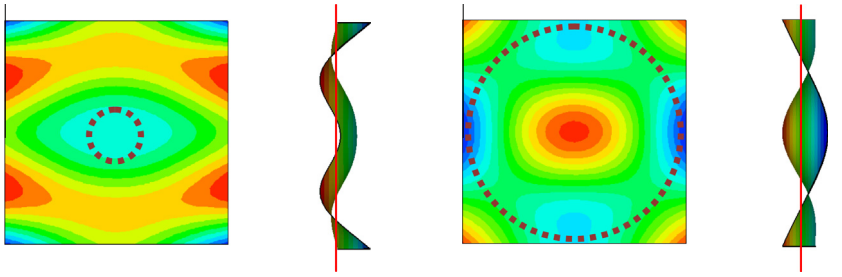	
920	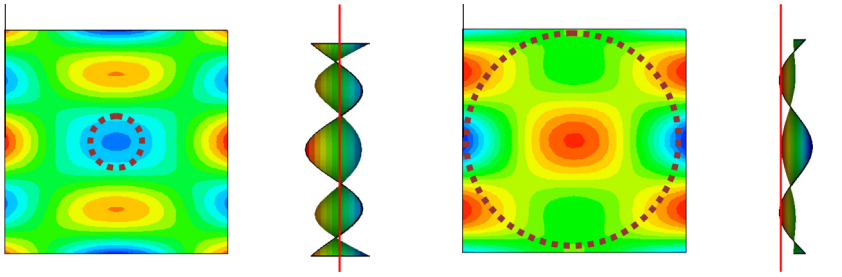	

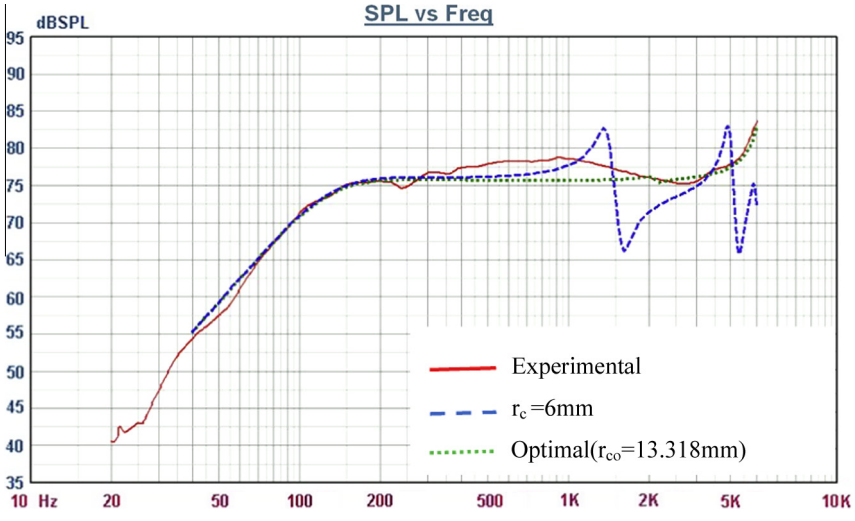

Fig. 8. SPL curve of Radiator B excited at different locations.

28.47 mm ($2r_{co}/b$ = 0.58) and 38.75 mm ($2r_{co}/b$ = 0.89), respectively. The SPL curves of the sound radiators with a/b = 1.25 and 1.6 are shown in Fig. 9 in comparison with the case with a/b = 1. It is noted that amongst the three cases under consideration, the case with a/b = 1.25 produces the smoothest SPL curve on which the dips are the smallest. Next, consider the effects of lamination arrangement on the optimal excitation location of Radiator A with a/b = 1. The optimal radii of the excitation locations for the sound radiators with layups of $[45°/-45°]_s$ and $[0°/90°]_s$ are 48.80 mm ($2r_{co}/b$ = 0.89) and 52.03 mm ($2r_{co}/b$ = 0.95), respectively. The SPL curves of the $[45°/-45°]_s$ and $[0°/90°]_s$ sound radiators are shown in Fig. 10 in comparison with the one of the original sound radiator with layup $[0°/0°]_s$. It is noted that amongst the three sound radiators, the one with the layup of $[45°/-45°]_s$ can produce a SPL

Table 2
Vibration shapes of Radiator B with different voice coil radii.

Frequency (Hz)	Mode shape	Vibration shape (r_c = 6 mm)	Vibration shape (r_{co} = 13.3 mm)
1600	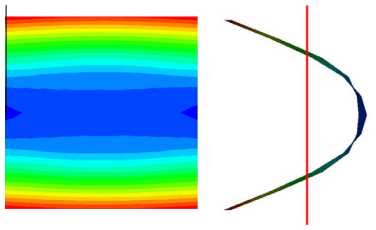	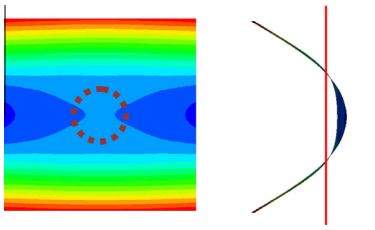	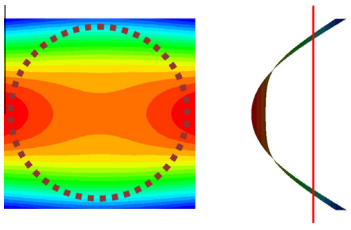
4200	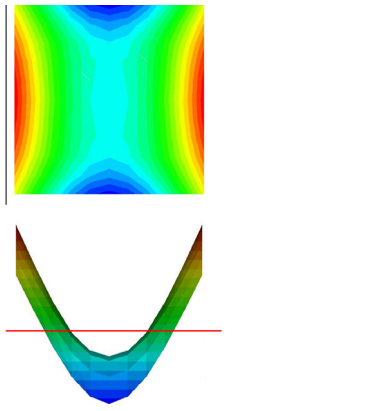	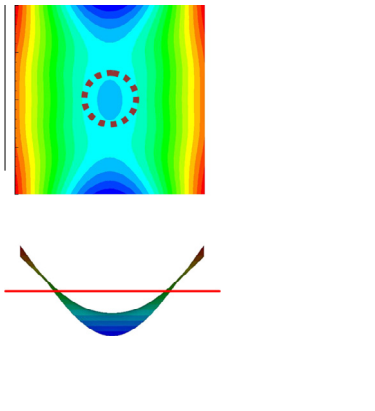	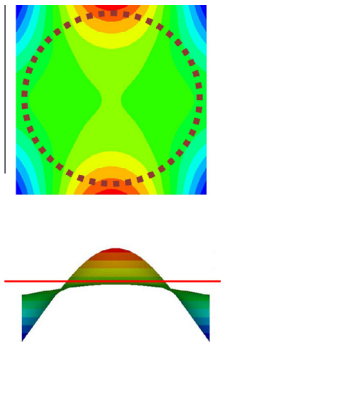

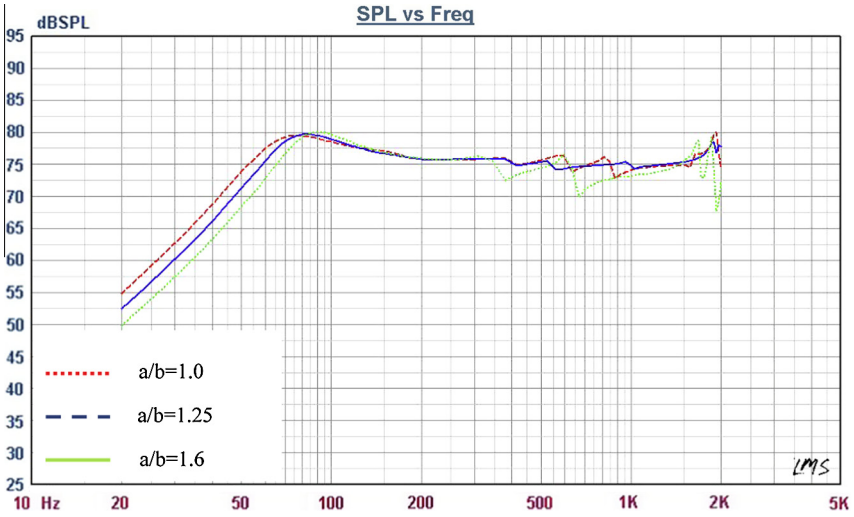

Fig. 9. SPL curves of Radiator A with different aspect ratios.

curve with the best smoothness. In particular, the major dip on the SPL curve of the $[45°/-45°]_s$ sound radiator becomes smaller and occurs in higher frequency range. In view of the above results for Radiator A with different aspect ratios and lamination arrangements, it is clear that both aspect ratio and lamination arrangement have significant effects on the smoothness of the SPL curve of a composite flat-panel sound radiator. Therefore, in addition to excitation location, aspect ratio and lamination arrangement should also be taken into consideration in the optimal design of composite flat-panel sound radiators.

7. Conclusion

An optimal design method has been proposed to design the optimal excitation locations for composite flat-panel sound radiators consisting of a circular exciter to obtain relatively smooth SPL curves in specific frequency ranges. The optimal design method consisting of three main parts, namely, the Rayleigh–Ritz method for vibration analysis, the Rayleigh first integral technique for sound radiation analysis, and a global optimization technique for determining the optimal excitation location, can solve the optimal design problem in an efficient and effective way. The proposed method has been used to design the excitation locations of several rectangular laminated composite flat-panel sound radiators with different aspect ratios and lamination arrangements. It has been shown that the sound radiators excited at the optimal locations can produce relatively smooth SPL curves. For the square $[0°]_4$, $[45°/-45°]_s$, and $[0°/90°]_s$ Carbon/Epoxy laminated composite sound radiators of length 110 mm, it has been shown that the ratios of optimal voice coil diameter to plate width are

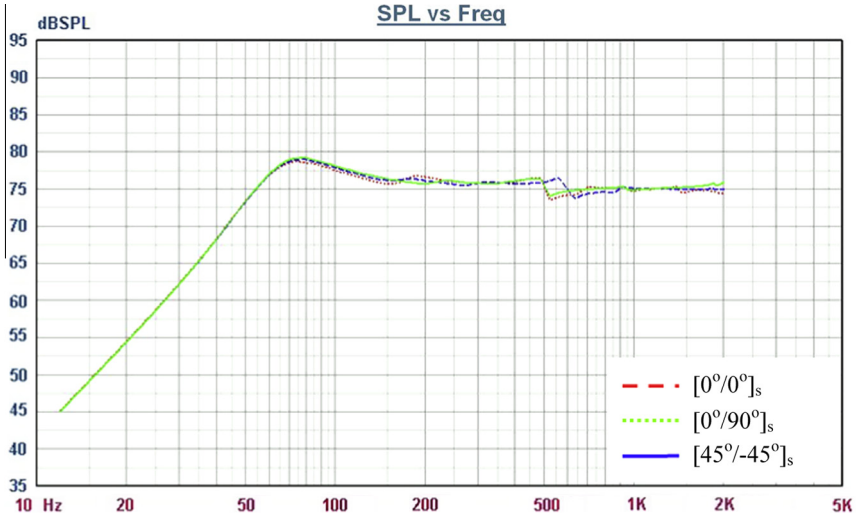

Fig. 10. Optimal SPL curves of Radiator A with different lamination arrangements.

$2r_{co}/b = 0.89$, 0.89, and 0.95, respectively, and comparatively the $[45°/-45°]_s$ sound radiator can produce the smoothest SPL curve. For the $[0°]_4$sound radiators with same area but different aspect ratios, it has been shown that the ratios of optimal voice coil diameter to plate width are $2r_{co}/b = 0.89$, 0.58, and 0.89, respectively, for aspect ratios $a/b = 1.0$, 1.25, and 1.6, respectively, and comparatively the sound radiator with $a/b = 1.25$ can produce the smoothest SPL curve. As for the square $[0°]_4$ sound radiators of size 30 mm, it has been shown that the ratio of optimal voice coil diameter to plate width is $2r_{co}/b = 0.89$ which is the same as that of the square sound radiator of length 110 mm. Furthermore, it has been shown that a relatively smooth SPL curve can be obtained if the excitation location is close to the nodal lines of the mode shapes that can induce SPL dips. Therefore, the role of the optimal excitation location is to minimize the adverse effects of the mode shapes that can induce SPL dips. The suitability of the optimal design method has also been validated by experimental results.

Acknowledgement

The work of this paper has been supported by the National Science Council of the Republic of China, Grant NSC 101-3113-S-009-002.

Appendix A

The elements of **K** and **M** are given in the following.

$$\left(\begin{bmatrix} K^{11} & K^{12} & K^{13} & 0 & 0 \\ K^{21} & K^{22} & K^{23} & K^{24} & K^{25} \\ K^{31} & K^{32} & K^{33} & K^{34} & K^{35} \\ 0 & K^{42} & K^{43} & K^{44} & K^{45} \\ 0 & K^{52} & K^{53} & K^{54} & K^{55} \end{bmatrix} - \omega^2 \begin{bmatrix} M^{11} & 0 & 0 & 0 & 0 \\ 0 & M^{22} & 0 & 0 & M^{25} \\ 0 & 0 & M^{33} & M^{34} & 0 \\ 0 & 0 & M^{43} & M^{44} & 0 \\ 0 & M^{52} & 0 & 0 & M^{55} \end{bmatrix}\right) \times \begin{Bmatrix} C_{ij} \\ C_{mn} \\ C_{pq} \\ C_{ab} \\ C_{cd} \end{Bmatrix} = \begin{Bmatrix} 0 \\ 0 \\ 0 \\ 0 \\ 0 \end{Bmatrix} \tag{A1}$$

with $N_b = N_t = 4$ and

$$\begin{aligned}
\left[K^{11}\right]_{ij\bar{i}\bar{j}} = {} & \left(\frac{4}{ab}A_{45}E^{10}_{i\bar{i}}F^{00}_{j\bar{j}} + \frac{4}{ab}A_{45}E^{01}_{i\bar{i}}F^{10}_{j\bar{j}} + \frac{8}{b^2}A_{44}E^{00}_{i\bar{i}}F^{11}_{j\bar{j}} + \frac{8}{a^2}A_{55}E^{11}_{i\bar{i}}F^{00}_{j\bar{j}}\right)\frac{ab}{8} \\
& + \frac{1}{2}(K_{L_1}bF^{00}_{j\bar{j}}[\phi_i(-1)\phi_{\bar{i}}(-1)] + K_{L_2}bF^{00}_{j\bar{j}}[\phi_i(1)\phi_{\bar{i}}(1)] \\
& + K_{L_3}aE^{00}_{i\bar{i}}[\phi_j(-1)\phi_{\bar{j}}(-1)] + K_{L_4}aE^{00}_{i\bar{i}}[\phi_j(1)\phi_{\bar{j}}(1)]) \\
& + K_CE^{00}_{i\bar{i}}F^{00}_{j\bar{j}} + \frac{2}{a}K_bG_bA_b\left(Bef^{11}_{j\bar{j}}Be^{00}_{i\bar{i}} + Bef^{11}_{j\bar{j}}Bf^{00}_{i\bar{i}}\right) \\
& + \frac{2}{b}K_bG_bA_b\left(Bc^{00}_{j\bar{j}}Bcd^{11}_{i\bar{i}} + Bd^{00}_{j\bar{j}}Bcd^{11}_{i\bar{i}}\right) \\
& + \frac{2}{a}K_mG_mA_m\left(Mef^{11}_{j\bar{j}}Me^{00}_{i\bar{i}} + Mef^{11}_{j\bar{j}}Mf^{00}_{i\bar{i}}\right) \\
& + \frac{2}{b}K_mG_mA_m\left(Mc^{00}_{j\bar{j}}Mcd^{11}_{i\bar{i}} + Md^{00}_{j\bar{j}}Mcd^{11}_{i\bar{i}}\right)
\end{aligned} \tag{A2}$$

$$\begin{aligned}
[K^{12}]_{ijmn} = {} & \left(\frac{2}{b}A_{45}E^{00}_{im}F^{01}_{jm} + \frac{4}{b}A_{55}E^{01}_{im}F^{00}_{jm}\right)\frac{ab}{8} \\
& + K_bG_bA_b\left(Bc^{00}_{jm}Bcd^{10}_{im} + Bd^{00}_{jm}Bcd^{10}_{im}\right) \\
& + K_mG_mA_m\left(Mc^{00}_{jm}Mcd^{10}_{im} + Md^{00}_{jm}Mcd^{10}_{im}\right)
\end{aligned}$$

$$\begin{aligned}
[K^{13}]_{ijpq} = {} & \left(\frac{2}{a}A_{45}E^{01}_{ip}F^{00}_{jq} + \frac{4}{a}A_{44}E^{00}_{ip}F^{01}_{jq}\right)\frac{ab}{8} \\
& + K_bG_bA_b\left(Bef^{10}_{jq}Be^{00}_{ip} + Bef^{10}_{jq}Bf^{00}_{ip}\right) \\
& + K_mG_mA_m\left(Mef^{10}_{jq}Me^{00}_{ip} + Mef^{10}_{jq}Mf^{00}_{ip}\right)
\end{aligned}$$

$$\begin{aligned}
[K^{22}]_{mn\bar{m}\bar{n}} = {} & \left(2A_{55}E^{00}_{m\bar{m}}F^{00}_{n\bar{n}} + \frac{8}{a^2}D_{11}E^{11}_{m\bar{m}}F^{00}_{n\bar{n}} + \frac{8}{ab}D_{16}E^{01}_{m\bar{m}}F^{10}_{n\bar{n}} + \frac{8}{ab}D_{16}E^{10}_{m\bar{m}}F^{01}_{n\bar{n}}\right. \\
& \left. + \frac{4}{b^2}D_{66}E^{00}_{m\bar{m}}F^{11}_{n\bar{n}}\right)\frac{ab}{8} \\
& + \left(\frac{h_p^2}{2b}E_bA_b + \frac{2h_b^2}{3b}E_bA_b + E_bh_pA_b\frac{h_b}{b}\right)\left(Bc^{00}_{n\bar{n}}Bcd^{11}_{m\bar{m}} + Bd^{00}_{n\bar{n}}Bcd^{11}_{m\bar{m}}\right) \\
& + \frac{b}{2}K_bG_bA_b\left(Bc^{00}_{n\bar{n}}Bcd^{00}_{m\bar{m}} + Bd^{00}_{n\bar{n}}Bcd^{00}_{m\bar{m}}\right) \\
& + \left(\frac{h_p^2}{2b}E_mA_m + \frac{2h_m^2}{3b}E_mA_m + E_mh_mA_m\frac{h_m}{b}\right) \\
& \times \left(Mc^{00}_{n\bar{n}}Mcd^{11}_{m\bar{m}} + Md^{00}_{n\bar{n}}Mcd^{11}_{m\bar{m}}\right) \\
& + \frac{b}{2}K_mG_mA_m\left(Mc^{00}_{n\bar{n}}Mcd^{00}_{m\bar{m}} + Md^{00}_{n\bar{n}}Mcd^{00}_{m\bar{m}}\right)
\end{aligned}$$

$$[K^{21}]_{mnij} = \left(\frac{4}{a}A_{55}E^{10}_{mi}F^{00}_{nj}\right)\frac{ab}{8}$$

$$[K^{23}]_{mnpq}=\left(\frac{8}{ab}D_{12}E^{01}_{mp}F^{10}_{nq}+\frac{8}{a^2}D_{16}E^{11}_{mp}F^{00}_{nq}+\frac{8}{b^2}D_{26}E^{00}_{mp}F^{11}_{nq}+\frac{4}{ab}D_{66}E^{10}_{mp}F^{01}_{nq}\right)\frac{ab}{8}$$

$$[K^{24}]_{mnab}=\left(\frac{8}{a^2}B_{11}E^{11}_{ma}F^{00}_{nb}+\frac{8}{ab}B_{16}E^{10}_{ma}F^{01}_{nb}+\frac{8}{ab}B_{16}E^{01}_{ma}F^{10}_{nb}+\frac{8}{b^2}B_{66}E^{00}_{ma}F^{11}_{nb}\right)\frac{ab}{8}$$

$$\begin{aligned}[K^{25}]_{mncd}=&\left(\frac{8}{a^2}B_{16}E^{11}_{mc}F^{00}_{nd}+\frac{8}{b^2}B_{26}E^{00}_{mc}F^{11}_{nd}+\frac{8}{ab}B_{12}E^{01}_{mc}F^{10}_{nd}\right)\frac{ab}{8}\\&+\left(\frac{h_p}{b}A_bE_b+\frac{h_b}{b}A_bE_b\right)\left(Bc^{00}_{nd}Bcd^{11}_{mc}+Bd^{00}_{nd}Bcd^{11}_{mc}\right)\\&-\left(\left(\frac{h_p}{b}A_mE_m+\frac{h_m}{b}A_mE_m\right)\left(Mc^{00}_{nd}Mcd^{11}_{mc}+Md^{00}_{nd}Mcd^{11}_{mc}\right)\right)\end{aligned}$$

$$\begin{aligned}[K^{33}]_{pq\overline{pq}}=&\left(2A_{44}E^{00}_{p\bar{p}}F^{00}_{q\bar{q}}+\frac{8}{b^2}D_{22}E^{00}_{p\bar{p}}F^{11}_{q\bar{q}}+\frac{8}{ab}D_{26}E^{10}_{p\bar{p}}F^{01}_{q\bar{q}}+\frac{8}{ab}D_{26}E^{01}_{p\bar{p}}F^{10}_{q\bar{q}}+\frac{8}{a^2}D_{66}E^{11}_{p\bar{p}}F^{00}_{q\bar{q}}\right)\frac{ab}{8}\\&+\left(\frac{h_p^2}{2a}E_bA_b+\frac{2h_b^2}{3a}E_bA_b+E_bh_pA_b\frac{h_b}{a}\right)\left(Bef^{11}_{q\bar{q}}Be^{00}_{p\bar{p}}+Bef^{11}_{q\bar{q}}Bf^{00}_{p\bar{p}}\right)\\&+\frac{a}{2}K_bG_bA_b\left(Bef^{00}_{q\bar{q}}Be^{00}_{p\bar{p}}+Bef^{00}_{q\bar{q}}Bf^{00}_{p\bar{p}}\right)\\&+\left(\frac{h_p^2}{2a}E_mA_m+\frac{2h_m^2}{3a}E_mA_m+E_mh_mA_m\frac{h_p}{a}\right)\left(Mef^{11}_{q\bar{q}}Me^{00}_{p\bar{p}}+Mef^{11}_{q\bar{q}}Mf^{00}_{p\bar{p}}\right)\\&+\frac{a}{2}K_mG_mA_m\left(Mef^{00}_{q\bar{q}}Me^{00}_{p\bar{p}}+Mef^{00}_{q\bar{q}}Mf^{00}_{p\bar{p}}\right)\end{aligned}$$

$$[K^{31}]_{pqij}=\left(\frac{2}{a}A_{45}E^{10}_{pi}F^{00}_{qj}+\frac{4}{b}A_{44}E^{00}_{pi}F^{10}_{qj}\right)\frac{ab}{8}$$

$$[K^{32}]_{pqmn}=\left(A_{45}E^{00}_{pm}F^{00}_{qn}+\frac{8}{ab}D_{12}E^{10}_{pm}F^{01}_{qn}+\frac{8}{a^2}D_{16}E^{11}_{pm}F^{00}_{qn}+\frac{8}{b^2}D_{26}E^{00}_{pm}F^{11}_{qn}+\frac{4}{ab}D_{66}E^{01}_{pm}F^{10}_{qn}\right)\frac{ab}{8}$$

$$\begin{aligned}[K^{34}]_{pqab}=&\left(\frac{8}{a^2}B_{16}E^{11}_{pa}F^{00}_{qb}+\frac{8}{b^2}B_{26}E^{00}_{pa}F^{11}_{qb}+\frac{8}{ab}B_{12}E^{10}_{pa}F^{01}_{qb}+\frac{8}{ab}B_{66}E^{01}_{pa}F^{10}_{qb}\right)\frac{ab}{8}\\&+\left(\frac{h_p}{a}A_bE_b+\frac{h_b}{a}A_bE_b\right)\left(Bef^{11}_{qb}Be^{00}_{pa}+Bef^{11}_{qb}Bf^{00}_{pa}\right)\\&-\left(\left(\frac{h_p}{a}A_mE_m+\frac{h_m}{a}A_mE_m\right)\left(Mef^{11}_{qb}Me^{00}_{pa}+Mef^{11}_{qb}Mf^{00}_{pa}\right)\right)\end{aligned}$$

$$[K^{35}]_{pqcd}=\left(B_{22}E^{00}_{pc}F^{00}_{qd}+\frac{8}{ab}B_{26}E^{10}_{pc}F^{01}_{qd}+\frac{8}{ab}B_{26}E^{01}_{pc}F^{10}_{qd}+\frac{8}{a^2}B_{66}E^{11}_{pc}F^{00}_{qd}\right)\frac{ab}{8}$$

$$\begin{aligned}[K^{44}]_{ab\overline{ab}}=&\left(\frac{8}{a^2}A_{11}E^{11}_{a\bar{a}}F^{00}_{b\bar{b}}+\frac{8}{ab}A_{16}E^{01}_{a\bar{a}}F^{10}_{b\bar{b}}+\frac{8}{ab}A_{16}E^{10}_{a\bar{a}}F^{01}_{b\bar{b}}+\frac{8}{b^2}A_{66}E^{00}_{a\bar{a}}F^{11}_{b\bar{b}}\right)\frac{ab}{8}\\&+\left(\frac{2}{a}E_bA_b\right)\left(Bef^{11}_{b\bar{b}}Be^{00}_{a\bar{a}}+Bef^{11}_{b\bar{b}}Bf^{00}_{a\bar{a}}\right)\\&+\left(\frac{2}{a}E_mA_m\right)\left(Mef^{11}_{b\bar{b}}Me^{00}_{a\bar{a}}+Mef^{11}_{b\bar{b}}Mf^{00}_{a\bar{a}}\right)\end{aligned}$$

$$[K^{42}]_{abmn}=\left(\frac{8}{a^2}B_{11}E^{11}_{am}F^{00}_{bn}+\frac{8}{ab}B_{16}E^{01}_{am}F^{10}_{bn}+\frac{8}{ab}B_{16}E^{10}_{am}F^{01}_{bn}+\frac{8}{b^2}B_{66}E^{00}_{am}F^{11}_{bn}\right)\frac{ab}{8}$$

$$[K^{43}]_{abpq}=\left(\frac{8}{a^2}B_{16}E^{11}_{ap}F^{00}_{bq}+\frac{8}{b^2}B_{26}E^{00}_{ap}F^{11}_{bq}+\frac{8}{ab}B_{12}E^{01}_{ap}F^{10}_{bq}+\frac{8}{ab}B_{66}E^{10}_{ap}F^{01}_{bq}\right)\frac{ab}{8}$$

$$[K^{45}]_{abcd}=\left(\frac{8}{a^2}A_{16}E^{11}_{ac}F^{00}_{bd}+\frac{8}{b^2}A_{26}E^{11}_{ac}F^{00}_{bd}+\frac{8}{ab}A_{12}E^{01}_{ac}F^{10}_{bd}+\frac{8}{ab}A_{66}E^{10}_{ac}F^{01}_{bd}\right)\frac{ab}{8}$$

$$\begin{aligned}[K^{55}]_{cd\overline{cd}}=&\left(\frac{8}{b^2}A_{22}E^{00}_{c\bar{c}}F^{11}_{d\bar{d}}+\frac{8}{ab}A_{26}E^{01}_{c\bar{c}}F^{10}_{d\bar{d}}+\frac{8}{ab}A_{26}E^{10}_{c\bar{c}}F^{01}_{d\bar{d}}+\frac{8}{a^2}A_{66}E^{11}_{c\bar{c}}F^{00}_{d\bar{d}}\right)\frac{ab}{8}\\&+\left(\frac{2}{b}E_bA_b\right)\left(Bc^{00}_{d\bar{d}}Bcd^{11}_{c\bar{c}}+Bd^{00}_{d\bar{d}}Bcd^{11}_{c\bar{c}}\right)\\&+\left(\frac{2}{b}E_mA_m\right)\left(Mc^{00}_{d\bar{d}}Mcd^{11}_{c\bar{c}}+Md^{00}_{d\bar{d}}Mcd^{11}_{c\bar{c}}\right)\end{aligned}$$

$$[K^{52}]_{cdmn}=\left(\frac{8}{a^2}B_{16}E^{11}_{cm}F^{00}_{dn}+\frac{8}{b^2}B_{26}E^{00}_{cm}F^{11}_{dn}+\frac{8}{ab}B_{12}E^{10}_{cm}F^{01}_{dn}+\frac{8}{ab}B_{66}E^{01}_{cm}F^{10}_{dn}\right)\frac{ab}{8}$$

$$[K^{53}]_{cdpq}=\left(\frac{8}{b^2}B_{22}E^{00}_{cp}F^{11}_{dq}+\frac{8}{ab}B_{26}E^{01}_{cp}F^{10}_{dq}+\frac{8}{ab}B_{26}E^{10}_{cp}F^{01}_{dq}+\frac{8}{a^2}B_{66}E^{11}_{cp}F^{00}_{dq}\right)\frac{ab}{8}$$

$$\begin{aligned}[K^{54}]_{cdab}=&\left(\frac{8}{a^2}A_{16}E^{11}_{ca}F^{00}_{db}+\frac{8}{b^2}A_{26}E^{00}_{ca}F^{11}_{db}+\frac{8}{ab}A_{12}E^{10}_{ca}F^{01}_{db}\right.\\&\left.+\frac{8}{ab}A_{66}E^{01}_{ca}F^{10}_{db}\right)\frac{ab}{8}\end{aligned}$$

and

$$\begin{aligned}[M^{11}]_{ij\overline{ij}}=&\left(\rho_ph_pE^{00}_{i\bar{i}}F^{00}_{j\bar{j}}\right)\frac{ab}{4}+\frac{a}{2}\rho_bA_b\left(Bef^{00}_{j\bar{j}}Be^{00}_{i\bar{i}}+Bef^{00}_{j\bar{j}}Bf^{00}_{i\bar{i}}\right)\\&+\frac{b}{2}\rho_bA_b\left(Bc^{00}_{j\bar{j}}Bcd^{00}_{i\bar{i}}+Bd^{00}_{j\bar{j}}Bcd^{00}_{i\bar{i}}\right)\\&+\frac{a}{2}\rho_mA_b\left(Mef^{00}_{j\bar{j}}Me^{00}_{i\bar{i}}+Mef^{00}_{j\bar{j}}Mf^{00}_{i\bar{i}}\right)\\&+\frac{b}{2}\rho_mA_m\left(Mc^{00}_{j\bar{j}}Mcd^{00}_{i\bar{i}}+Md^{00}_{j\bar{j}}Mcd^{00}_{i\bar{i}}\right)\end{aligned}\tag{A3}$$

$$\begin{aligned}[M^{22}]_{mn\overline{mn}}=&\left(\rho_p\frac{h_p^3}{12}E^{00}_{m\bar{m}}F^{00}_{n\bar{n}}\right)\frac{ab}{4}\\&+\left(\frac{h_p^2b}{8}\rho_bA_b+\frac{h_b^2b}{6}\rho_bA_b+\frac{h_bb}{4}\rho_bA_b\right)\left(Bc^{00}_{n\bar{n}}Bcd^{00}_{m\bar{m}}+Bd^{00}_{n\bar{n}}Bcd^{00}_{m\bar{m}}\right)\\&+\left(\frac{h_p^2b}{8}\rho_mA_m+\frac{h_m^2b}{6}\rho_mA_m+\frac{h_mb}{4}\rho_mA_m\right)\left(Mc^{00}_{n\bar{n}}Mcd^{00}_{m\bar{m}}+Md^{00}_{n\bar{n}}Mcd^{00}_{m\bar{m}}\right)\end{aligned}$$

$$\begin{aligned}[M^{25}]_{mncd}=&\left(b\rho_bA_b\frac{h_p}{4}+b\rho_bA_b\frac{h_b}{4}\right)\left(Bc^{00}_{nd}Bcd^{00}_{mc}+Bd^{00}_{nd}Bcd^{00}_{mc}\right)\\&-\left(b\rho_mA_m\frac{h_p}{4}+b\rho_mA_m\frac{h_m}{4}\right)\left(Mc^{00}_{nd}Mcd^{00}_{mc}+Md^{00}_{nd}Mcd^{00}_{mc}\right)\end{aligned}$$

$$\begin{aligned}[M^{33}]_{pq\overline{pq}}=&\left(\rho_p\frac{h_p^3}{12}E^{00}_{p\bar{p}}F^{00}_{q\bar{q}}\right)\frac{ab}{4}\\&+\left(\frac{h_p^2a}{8}\rho_bA_b+\frac{h_b^2a}{6}\rho_bA_b+\frac{h_ba}{4}\rho_bA_b\right)\left(Bef^{00}_{q\bar{q}}Be^{00}_{p\bar{p}}+Bef^{00}_{q\bar{q}}Bf^{00}_{p\bar{p}}\right)\\&+\left(\frac{h_p^2a}{8}\rho_mA_m+\frac{h_m^2a}{6}\rho_mA_m+\frac{h_ma}{4}\rho_mA_m\right)\left(Mef^{00}_{q\bar{q}}Me^{00}_{p\bar{p}}+Mef^{00}_{q\bar{q}}Mf^{00}_{p\bar{p}}\right)\end{aligned}$$

$$\begin{aligned}[M^{34}]_{pqab}=&\left(a\rho_bA_b\frac{h_p}{4}+a\rho_bA_b\frac{h_b}{4}\right)\left(Bef^{00}_{qb}Be^{00}_{pa}+Bef^{00}_{qb}Bf^{00}_{pa}\right)\\&-\left(a\rho_mA_m\frac{h_p}{4}+a\rho_mA_m\frac{h_m}{4}\right)\left(Mef^{00}_{qb}Me^{00}_{pa}+Mef^{00}_{qb}Mf^{00}_{pa}\right)\end{aligned}$$

$$\begin{aligned}[M^{44}]_{ab\overline{ab}}=&\left(\rho_ph_pE^{00}_{a\bar{a}}F^{00}_{b\bar{b}}\right)+\left(\frac{a}{2}\rho_bA_b\right)\left(Bef^{00}_{b\bar{b}}Be^{00}_{a\bar{a}}+Bef^{00}_{b\bar{b}}Bf^{00}_{a\bar{a}}\right)\\&+\left(\frac{a}{2}\rho_mA_m\right)\left(Mef^{00}_{b\bar{b}}Me^{00}_{a\bar{a}}+Mef^{00}_{b\bar{b}}Mf^{00}_{a\bar{a}}\right)\end{aligned}$$

$$\begin{aligned}[M^{55}]_{cd\overline{cd}}=&\left(\rho_ph_pE^{00}_{c\bar{c}}F^{00}_{d\bar{d}}\right)+\left(\frac{b}{2}\rho_bA_b\right)\left(Bc^{00}_{d\bar{d}}Bcd^{00}_{c\bar{c}}+Bd^{00}_{d\bar{d}}Bcd^{00}_{c\bar{c}}\right)\\&+\left(\frac{b}{2}\rho_mA_m\right)\left(Mc^{00}_{d\bar{d}}Mcd^{00}_{c\bar{c}}+Md^{00}_{d\bar{d}}Mcd^{00}_{c\bar{c}}\right)\end{aligned}$$

where

$$\begin{aligned}&r,s=0,1;\quad i,j,\bar{i},\bar{j}=1,2,3,\ldots I,J\\&m,n,\bar{m},\bar{n}=1,2,3,\ldots M,N\\&p,q,\bar{p},\bar{q}=1,2,3,\ldots P,Q\\&a,b,\bar{a},\bar{b}=1,2,3,\ldots A,B\\&c,d,\bar{c},\bar{d}=1,2,3,\ldots C,D\end{aligned}\tag{A4}$$

$$E_{im}^{rs}=\int_{-1}^{1}\left[\frac{d^r\phi_i(\xi)}{d\xi^r}\frac{d^s\phi_m(\xi)}{d\xi^s}\right]d\xi;\quad F_{jn}^{rs}=\int_{-1}^{1}\left[\frac{d^r\phi_j(\eta)}{d\eta^r}\frac{d^s\phi_n(\eta)}{d\eta^s}\right]d\eta$$

$$Bcd_{im}^{rs}=\int_{-\frac{L_2}{a}}^{\frac{L_2}{a}}\phi_i^r(\xi)\phi_m^s(\xi)d\xi;\quad Mcd_{im}^{rs}=\int_{-\frac{L_2}{a}}^{\frac{L_2}{a}}\phi_i^r(\xi)\phi_m^s(\xi)d\xi$$

$$Bef_{im}^{rs}=\int_{-\frac{L_1}{b}}^{\frac{L_1}{b}}\varphi_i^r(\eta)\phi_m^s(\eta)d\eta;\quad Mef_{im}^{rs}=\int_{-\frac{L_1}{b}}^{\frac{L_1}{b}}\varphi_i^r(\eta)\varphi_m^s(\eta)d\eta$$

$$Bc_{im}^{rs}=\phi_i^r(\xi=\frac{-L_2}{a})\phi_m^s\left(\xi=\frac{-L_2}{a}\right);\ Bd_{im}^{rs}=\phi_i^r\left(\xi=\frac{L_2}{a}\right)\phi_m^s\left(\xi=\frac{L_2}{a}\right)$$

$$Be_{im}^{rs}=\phi_i^r\left(\eta=\frac{-L_1}{b}\right)\varphi_m^s\left(\eta=\frac{-L_1}{b}\right);\ Bf_{im}^{rs}=\varphi_i^r\left(\eta=\frac{L_1}{b}\right)\varphi_m^s\left(\eta=\frac{L_1}{b}\right)$$

$$Mc_{im}^{rs}=\phi_i^r\left(\xi=\frac{-L_2}{a}\right)\phi_m^s\left(\xi=\frac{-L_2}{a}\right);\ Md_{im}^{rs}=\phi_i^r\left(\xi=\frac{L_2}{a}\right)\phi_m^s\left(\xi=\frac{L_2}{a}\right)$$

$$Me_{im}^{rs}=\varphi_i^r\left(\eta=\frac{-L_1}{b}\right)\varphi_m^s\left(\eta=\frac{-L_1}{b}\right);\ Mf_{im}^{rs}=\phi_i^r\left(\eta=\frac{L_1}{b}\right)\varphi_m^s\left(\eta=\frac{L_1}{b}\right)\tag{A5}$$

References

[1] Guenther EW. Leigh S. Flat-panel speaker. US 5701359; 1997.
[2] Bertagni A, Bertagni E, Schuessler J, Ferrin A. Planar diaphragm loudspeaker with counteractive weights. US5615275; 1997.
[3] NEC Corp. Panel speaker with wide free space. US6554098; 2000.
[4] Azima H, Colloms M, Harris NJ. Panel-form loudspeakers. US6031926; 2000.
[5] Kam TY. Rectangular panel-form loudspeaker and its radiating panel. US7010143; 2006.
[6] Kam TY. Transparent panel-form loudspeaker. US7110561B2; 2006.
[7] Kam TY. Moving-coil planar speaker. US8085971; 2011.
[8] Sargianis JJ, Kim HI, Andres E, Jonghwan S. Sound and vibration damping characteristics in natural material based sandwich composites. J Compos Struct 2013;96:538–44.
[9] Putra A, Thompson DJ. Radiation efficiency of unbaffled and perforated plates near a rigid reflecting surface. J Sound Vib 2011;330(22):5443–59.
[10] Kam TY, Jiang CH, Lee BY. Vibro-acoustic formulation of elastically restrained shear deformable stiffened rectangular plate. J Compos Struct 2012;94:3132–41.
[11] Inalpolat M, Caliskan M, Sing R. Analysis of near field sound radiation from a resonant unbaffled plate using simplified analytical models. Noise Control Eng J 2010;58(2):145–56.
[12] Larbi W, Deue J-F, Ohayon R. Finite element formulation of smart piezoelectric composite plates coupled with acoustic fluid. J Compos Struct 2012;94(2):501–9.
[13] Sorokin SV. Vibrations of and sound radiation from sandwich plates in heavy fluid loading conditions. J Compos Struct 2000;48(4):219–30.
[14] Zhang X, Li WL. A unified approach for predicting sound radiation from baffled rectangular plates with arbitrary boundary. J Sound Vib 2010;329(25):5307–20.
[15] Xing YF, Liu B. New exact solutions for free vibrations of thin orthotropic rectangular plates. J Compos Struct 2009;89(4):567–74.
[16] Cao X, Hua H, Zhang Z. Sound radiation from shear deformable stiffened laminated plates. J Sound Vib 2011;330:4047–63.
[17] Lomas NS, Hayek SI. Vibration and acoustic radiation of elastically supported rectangular plates. J Sound Vib 1977;52(1):1–25.
[18] Berry A, Guyader JL, Nicolas J. A General formulation for the sound radiation from rectangular baffled plates with arbitrary boundary conditions. J Acoust Soc Am 1990;88(6):2792–802.
[19] Yoo JW. Study on the general characteristics of the sound radiation of a rectangular plate with different boundary edge conditions. J Mech Sci Technol 2010;24(5):1111–8.
[20] Li WL. Vibro-acoustic analysis of rectangular plates with elastic rotational edge restraints. J Acoust Soc Am 2006;120(2):769–79.
[21] Zhang SZ, Shen Y, Shen XX, Zhou JL. Model optimization of distributed-mode loudspeaker using attached masses. J Audio Eng Soc 2006;54:295–305.
[22] Lu G, Shen Y. Model optimization of orthotropic distributed-mode loudspeaker using attached masses. J. Acoust Soc Am 2009;126:2294–300.
[23] Kam TY, Jiang CH, Hsu KJ. Vibro-acoustics of flat-panel speakers with attached lumped masses. Recent Patents Mech Eng 2012;5:194–207.
[24] Lu G, Shen Y, Liu Z. Optimization of orthotropic distributed-mode loudspeaker using attached masses and multi-exciters. J Acoust Soc Am 2012;131:93–8.
[25] Yin XW, Cui HF. Acoustic radiation from a laminated composite plate excited by longitudinal and transverse mechanical drives. J Appl Mech 2009;76(4):044501–5.
[26] Mindlin RD. Influence of rotatory inertia and shear on flexural motions of isotropic, elastic panels. J Appl Mech 1951;18:31–8.
[27] Ochoa OO, Reddy JN. Finite element analysis of composite laminates. The Netherlands: Kluwer; 1992.
[28] Whitney JM. Shear correction factors for orthotropic laminates under static load. J Appl Mech 1973;40:302–4.
[29] Kam TY, Chang RR. Finite element analysis of shear deformable laminated composite plates. ASME J Energy Resour Technol 1993;115:41–6.
[30] Kam TY, Chang RR. Buckling of shear deformable laminated composite plates. J Compos Struct 1992;22:223–34.
[31] Kam TY, Chang RR. Impact analysis of shear deformable laminated composite plates. ASME J Energy Resour Technol 1995;117:219–27.
[32] Snyman JA, Fatti LP. A multi-start global minimization algorithm with dynamic search trajectories. J Optim Theory Appl 1987;54(1):121–41.
[33] Wang WT, Kam TY. Determination of elastic constants of composite laminates via static testing. J Compos Struct 2000;50(4):347–52.
[34] Kam TY, Lai FM. Maximum stiffness design of laminated composite plates via a constrained global optimization approach. J Compos Struct 1995;32(1):391–8.
[35] LMS, version 4; 2010.
[36] ANSYS 12.1, ANSYS, Inc., USA; 2010.
[37] Jiang CH. Vibro-acoustics of elastically restrained composite sound radiators. PhD dissertation, Mechanical Engineering Department, National Chiao Tung University, Hsin Chu, Taiwan; 2013 [in Chinese].